Microporous and Mesoporous Materials 317 (2021) 110988

Contents lists available at ScienceDirect

Microporous and Mesoporous Materials

journal homepage: http://www.elsevier.com/locate/micromeso

Structural changes in resorcinol formaldehyde aerogel seen by NMR

Mónika Kéri [a,*], Balázs Nagy [b], Krisztina László [b], István Bányai [a]

[a] University of Debrecen, Department of Physical Chemistry, H-4032, Debrecen, Egyetem tér 1, Hungary
[b] Budapest University of Technology and Economics, Department of Physical Chemistry and Materials Science, H-1521, Budapest, PO Box 91, Hungary

ARTICLE INFO

Keywords:
Resorcinol-formaldehyde aerogel
Carbon aerogel
Pore morphology
NMR cryoporometry

ABSTRACT

Carbon aerogels prepared from resorcinol formaldehyde organic aerogels have a wide range of use due to their considerably large specific surface area. Since the applications mostly happen in wet form, e.g. in aqueous medium, NMR cryoporometry was employed to follow the porous behavior of an organic aerogel and its carbon derivative, as well as the textural changes after the pyrolysis. Water and cyclohexane were used as hydrophilic and hydrophobic probe molecules, respectively. In the polymer aerogel, saturated with water, by NMR we found spherical mesopores confined by the aerogel beads and wide channels in the macropore size-range separating the aggregated beads. After carbonization cylindrical pores were observed between the beads and the aggregates got closer to each other. On the other hand, the hydrophobic cyclohexane probed exclusively the macropores, which might be the result of local swelling. The micropore region both in the polymer and the carbonized form was explored only by the low temperature gas adsorption measurements. The comparison of the two methods confirmed that these techniques excellently complement each other in characterizing the micro-, meso- and macropores of solid porous materials: vapor adsorption is superior in characterizing the micro- and mesoporosity, while NMR cryoporometry provides information about the pore geometry and size distribution in the meso- and macropores.

1. Introduction

Resorcinol formaldehyde (RF) aerogels have many excellent properties such as large specific surface area and tunable porosity [1–3]. Furthermore, RF polymer aerogels are also precursors of carbon aerogels, which are relatively good electric conductors due to the carbon matrix and heat insulators as a result of their porosity. Therefore these materials attract great attention in adsorption, catalysis, energy storage, and conversion applications [4]. Their applications in energy storage devices (lithium ion batteries, supercapacitors, fuel cells, etc.) are widely studied [5–8]. The open, interconnected pore network of micro-, meso- and macropores, which can be tuned by the conditions of the synthesis, drying and carbonization of the polymer aerogel, makes these materials extremely high capacity adsorbents as well [9–12].

RF based carbon aerogels are obtained after the pyrolysis of the RF polymer aerogels. During the polymer to carbon conversion also the texture of the aerogel undergoes important changes. The microporosity generally increases, resulting in an increase of the apparent surface area. On the other hand, the alterations in the meso- and macropore regions may be more sensitively affected by the experimental conditions [13–16]. Gas adsorption methods are the most widely used vehicles for the characterization of the porosity and pore size distribution. Electron microscopic methods, scattering (e.g., SAXS and SANS), and various spectroscopies can be used to complete the textural and, occasionally, the surface chemical information [17]. Most of these techniques provide information about the solid sample in evacuated conditions. However, the above-mentioned applications take place in a solvent, mostly aqueous medium. Therefore, from the application point of view, the investigation of the porous structure in liquid medium is essential. Recently, nuclear magnetic resonance (NMR) cryoporometry has appeared more frequently in the literature for characterizing the pore shape and size [18–25]. It takes advantage of the melting and freezing point depressions of liquids confined in pores. Water and organic solvents (e.g., cyclohexane) are often used as probe liquids depending on the character of the porous matrix. While the RF polymer aerogels contain phenolic hydroxyl groups, their pyrolysis results in carbon aerogels of a more hydrophobic character. However, the skeleton of carbon aerogels is often decorated with hydrophilic functional groups.

* Corresponding author. Department of Physical Chemistry, H-4032, Debrecen, Egyetem tér 1, Hungary.
E-mail addresses: keri.monika@science.unideb.hu (M. Kéri), nagy.b555@gmail.com (B. Nagy), klaszlo@mail.bme.hu (K. László), banyai.istvan@science.unideb.hu (I. Bányai).

https://doi.org/10.1016/j.micromeso.2021.110988
Received 1 December 2020; Received in revised form 20 January 2021; Accepted 13 February 2021
Available online 24 February 2021

Cadar et al. compared the wetting of carbon xero- and aerogels in water and cyclohexane. They observed a non-uniform water distribution, while the cyclohexane forms a uniform, strongly attached surface layer [26,27]. On this basis, we assume that cryoporometry measurements carried out with both liquids (water and cyclohexane) can give extra information about the pore structure compared to the conventional methods.

NMR cryoporometry has already been applied in the case of carbon-based materials. Ghosh et al. [28] investigated the freezing of water inside carbon nanotubes of 1.4 nm diameter by NMR cryoporometry, and were able to distinguish water inside the nanotube and adsorbed on the wall. It must be noted that their cryoporometry experiments were made far out of the so-called large pore limit, where the quantitative evaluation of the data is possible [23]. Zhao et al. found correlating NMR cryoporometry and nitrogen adsorption pore size distribution curves for coal samples [29]. Krutyeva et al. combined gas adsorption, NMR cryoporometry, and some other NMR methods to characterize carbon molecular sieves and activated carbons [30]. They systematically built up a characterization protocol as follows: the specific surface area and the porosity were accepted from the gas sorption, while the pore size distribution from the NMR cryoporometry on samples, completely saturated with nitrobenzene.

The aim of our work was to determine the morphology of an RF polymer aerogel (PA) and the derived carbon aerogel (CA) in liquid media, and to study the applicability of NMR cryoporometry to follow the textural changes during the pyrolysis process. The texture of the aerogels was characterized by NMR cryoporometry, nitrogen and water vapor adsorption as well as scanning electron microscopy (SEM) to reveal the compatibility of the methods. Cryoporometry measurements were carried out in aqueous and cyclohexane media to understand the role of the polarity of the probe liquids.

2. Experimental

2.1. Synthesis of the aerogels

The aerogel samples were prepared similarly to the first reported synthesis of polymer and carbon aerogels [31]. Briefly, first a resorcinol (R)-formaldehyde (F) hydrogel was prepared with an R/catalyst (Na_2CO_3) mass ratio of 50. After changing the water to acetone, the wet gel was dried in supercritical CO_2 yielding the polymer aerogel, PA (48%) [32]. The dry gel was converted to carbon aerogel, CA, in a rotary quartz reactor at 1173 K for 1 h in a 25 mL/min high purity nitrogen flow (99.996%, Linde). The preparation process is summarized in Fig. 1.

2.2. Characterization

Scanning and transmission electron microscopy (SEM and TEM, respectively) were used for taking the image of the texture (Hitachi SU8030 and JEM2011).

Low temperature nitrogen adsorption measurements (77 K) were carried out with a NOVA 2000e (Quantachrome) automatic volumetric gas sorption analyzer instrument to determine the surface area and pore size distributions of the aerogels. The BET model was used to obtain the apparent surface area from the isotherms [33]. The volume of micropores was derived from the Dubinin-Radushkevich (DR) model [34]. As no kernel files, necessary for DFT based calculations, are available for polymers, the pore size distributions were calculated with the Barrett, Joyner and Halenda (BJH) model [35]. The use of this model limits the window of the pore size distribution curves. The pore size distribution of the carbon gel was calculated with the NLDFT equilibrium model. The best fit (fitting error 0.65%) was obtained with slit-like pore geometry. Data evaluation was carried out with the software of the manufacturer of the instrument (ASiQwin version 3.0).

Water vapor sorption was applied for the hydrophilic/hydrophobic characterization. The isotherm was measured on a static volumetric Hydrosorb (Quantachrome) water vapor sorption analyzer at 293 K.

2.3. NMR experiments and data evaluation

NMR cryoporometry is used for determining the pore size distribution of wetted porous materials. Since this technique is less known, we briefly introduce its theoretical background in the following.

Cryoporometry is based on the phenomena that liquids in a confined geometry (=pore) melt and freeze at lower temperatures ($T_{m/f}$) than in the bulk phase (T_0) [36]. By liquid-phase NMR only the molten phase is detected, thus the melting and freezing processes can be followed through the detected intensity of the NMR signal by changing the temperature. Using a modified form of the Gibbs-Thompson equation (eq. (1)) the pore size and pore size distribution can be calculated [37].

$$\Delta T_{m/f} = T_{m/f} - T_0 = -\frac{nK_c}{r_p} \quad (1)$$

where n is a factor characteristic for the pore geometry, K_c is the cryoporometric constant of the liquid, and r_p is the radius for spherical and cylindrical pores, and the half-distance between planar surfaces [23]. n is 3, 2 and 1 for spherical, cylindrical and slit-shaped geometry respectively for the freezing, while 2, 1, and 0 for the melting process. It is obtained from the different mechanism of freezing and melting, if no special bottle-effect or uncontrollable delay by nucleation occurs on cooling. It means that in certain cases a hysteresis can be observed on the freezing-melting curves [22–25]. The NMR pore size distributions are often compared favorably with gas adsorption results; nevertheless gas adsorption data are occasionally used for the calibration of the NMR methods [30,39]. When the gas sorption and cryoporometric experiments give different results, either of them can be correct but holds different or complementary information. With careful interpretation, they can turn the results more reliable.

Cryoporometric experiments were carried out on the RF polymer aerogel (PA) and its carbon derivative (CA) fully saturated with the probe liquids. The gels were introduced into plastic NMR tubes and loaded with deionized (Milli-Q) water. In the case of CA, cyclohexane (AnalaR NORMAPUR® ACS, Reag. Ph. Eur) was also used as probe

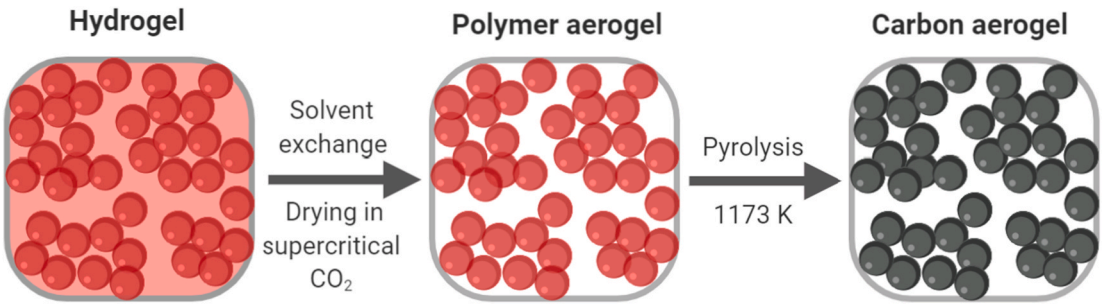

Fig. 1. Scheme of the preparation of RF polymer and carbon aerogels from hydrogel.

liquid. Before the NMR experiment, we waited at least one day for the diffusion of the liquid into the aerogels. After the calibration of several parameters (90° pulse length, echo time, *etc.*) the samples were frozen at 233 K. Dried, cold air and a cooling unit (BSCU 05) was used for cooling the probe head (400 MHz inverse broadband probe head). The temperature was changed from 264 K to about 274 K for water and to 282 K for cyclohexane filled samples and ^{1}H spectra were recorded at every 0.1, 0.2 or 0.5 K step after a temperature equilibration of 5 min. The thermometer was previously calibrated against ethylene glycol and methanol [40]. The temperature calibration was also confirmed by the bulk transition temperature of the probe liquids. The ^{1}H NMR spectrum of the sample was recorded by a spin echo sequence to eliminate the broad signal of the frozen liquid during the echo time, which was typically 0.5–1 ms [23]. MestReNova 9.0© was used for the post-processing. To follow the melting and freezing processes the peak integrals of the molten liquid were plotted as a function of the temperature. From the melting-freezing hysteresis the pore geometry was deduced and according to eq. (1) pore radii were calculated. The K_c was taken as 30 nm K for water and 96 nm K for cyclohexane according to Petrov and Furo [23]. The pore size distribution curves were plotted after the numerical derivation of the integral - pore radius function in the following way: the measured data were fitted with asymmetric logistic curves (like Richards and Gompertz growth functions) using the OriginPro 8.6© software and the analytical derivatives were calculated [41].

3. Results and discussion

3.1. Morphology of the aerogels seen by vapor adsorption

The electron microscopic images of the aerogels are shown in Fig. 2, revealing the presence of pores in a wide size range as well as their interconnected nature. The size of the beads is about 30 nm in the polymer and 12 ± 3 nm in the carbon aerogel.

The morphology of PA and CA was characterized by low temperature N_2 adsorption measurements. Fig. 3 shows the adsorption isotherms and the pore size distributions (diameter, d) derived from both the adsorption and desorption branches. As no kernel file is available for polymer samples necessary for DFT based calculations, we used the BJH model for the sake of comparison.

The nitrogen adsorption/desorption isotherms of the aerogels are of type IV(a) according to the IUPAC classification revealing an interconnected pore network of aggregated particles [42]. Although the PA contains micropores, wider mesopores and macropores dominates its porosity. After the pyrolysis the type of the isotherm conserved, however, due to the thermal treatment of the polymer beads the contribution of the micropores significantly increased. The isotherms have a hysteresis loop of type H3, *i.e.*, the pore network also contains macropores not completely filled with liquid nitrogen. Their size, as seen by SEM/TEM, exceeds the upper limit of the nitrogen adsorption technique. The closure point of the loops, marking the cavitation induced evaporation is at ca p/p_0 0.65 in the polymer and is shifted to 0.75 after the pyrolysis.

The SEM images and the shape of the isotherms confirm the textural similarity of PA and CA. The isotherm is practically shifted upward as a result of the pyrolysis. The most significant change is an intensive increase occurring in the microporous region. The opposite trend in the total pore volume (Fig. 3 and Table 1.) can be explained by the limits of the nitrogen adsorption technique. The enhanced microporosity also leads to the increase of the apparent surface area and a more than 50% drop of the average pore size (d_{ave}) detected by this technique (Table 1.). The comparison of the pore size distributions calculated from the corresponding branches of the isotherms confirms that the pyrolytic heat treatment does not alter the pore size distribution in the mesopore range [10,43]. The DFT based pore size distribution of CA (Fig. 3b, inset) reveals the existence of micropores in the 1–2 nm range and confirms the presence of the mesopores seen in the BJH distribution.

Water vapor adsorption of the carbon aerogel provides information about the hydrophilic/hydrophobic character of the porous material. It is important to know, that XPS analysis revealed that the surface contains 5.4 atomic % O, 49.1% of which is in C═O and 47.6% in R–OH or R-O-R forms [44]. Indeed, the initial slope of the water vapor isotherm of the carbon gel (Fig. 4) shows that the surface of the carbon contains enough polar groups to adsorb water even at low relative humidity.

3.2. Morphology of the aerogels seen by NMR

The pore structure of PA immersed in water was studied by NMR cryoporometry. The expected results allow to test the potential morphological changes in water and the compatibility of the adsorption and NMR methods. Fig. 5a shows the freezing and melting processes of water in the saturated polymer aerogel. The two overlapping melting curves (empty symbols in Fig. 5a) show the good reproducibility of the experiment. The molten water appears first at around 266 K, and a melting process shows up in a wide temperature range up to 271 K with an inflexion point at about 269.5 K. This melting is accompanied by a freezing step between 269 and 264 K, showing an inflexion point at 267.8 K. The ratio of the freezing (ΔT_f = 5.35 K) and melting point depression (ΔT_m = 3.65 K) equals 1.5, which coincides with the spherical pore geometry model in the large pore limit according to Petrov and Furo [23].

The second sharp melting step around 273.2 K belongs to bulk water. The corresponding freezing process is shifted to ca. 272 K. Considering some theoretical arguments of Petrov and Furo [23,24], like the influence of the pore geometry and pore wall curvature on the freezing-melting hysteresis, this effect is characteristic for slit-like pores. It means a spatial dimension being infinite in two directions (at least in the size-range of NMR cryoporometry) and finite in one direction, thus can be interpreted as a wide channel as well. The ratio of the signal integral of the two freezing steps indicates the distribution of pore water in the different pore types, namely that ca. 11% of water is located in the

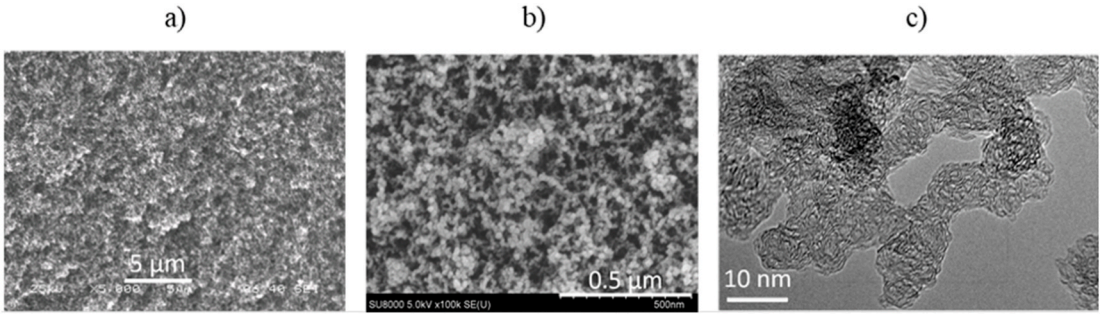

Fig. 2. SEM and HRTEM images of the aerogels. a) SEM of the polymer aerogel, the scale bar is 5 µm. b) SEM and c) HRTEM of the carbon sample. The scale bars are 0.5 µm and 10 nm, respectively.

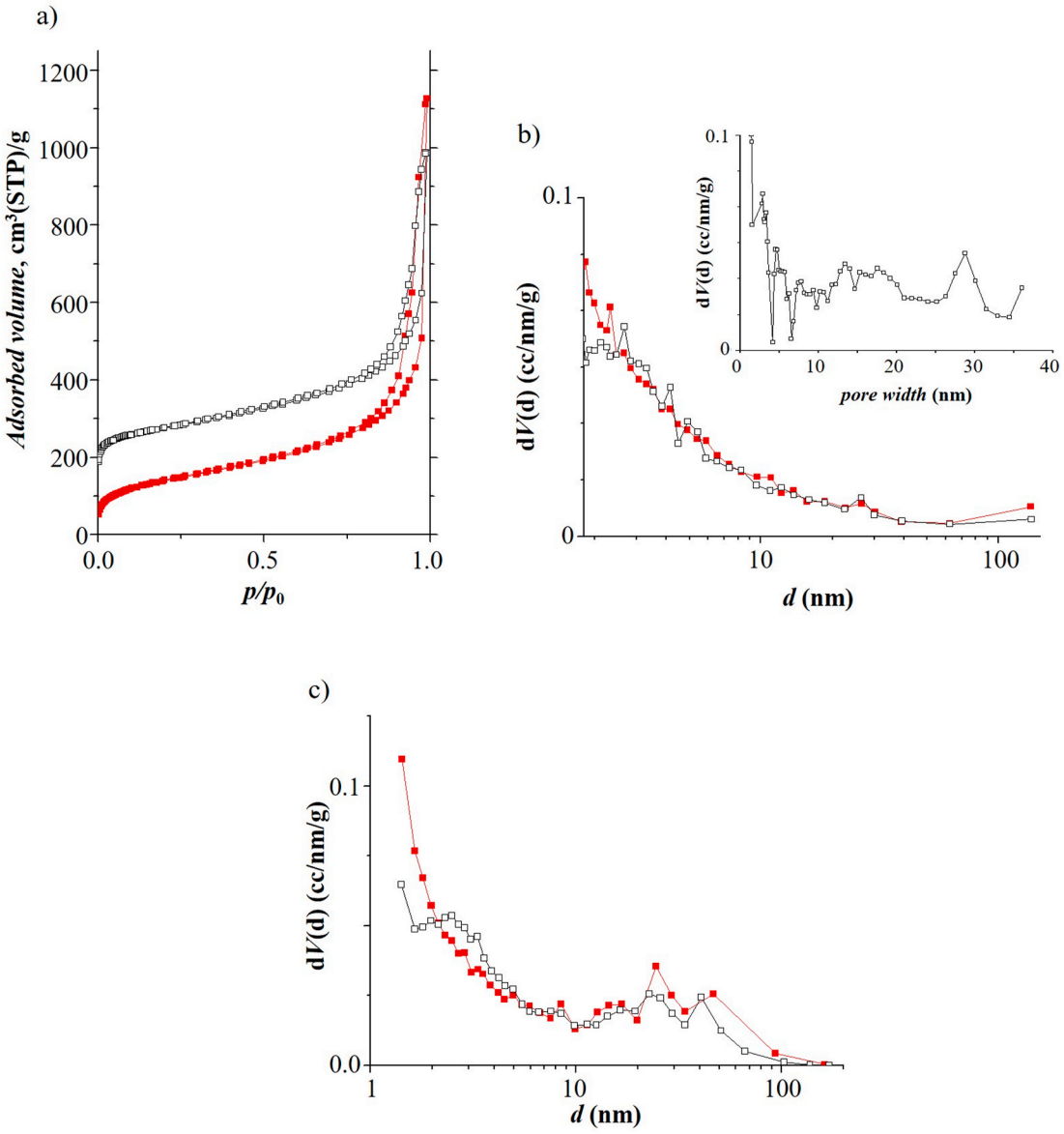

Fig. 3. a) Low temperature nitrogen adsorption/desorption isotherms; b) semi-logarithmic plot of pore size distribution from the adsorption and c) desorption branches calculated with the BJH model. The inset of b) shows the linear plot from NLDFT calculation for slit-shaped pores. Full symbols (red): PA, open symbols (black): CA. (For interpretation of the references to colour in this figure legend, the reader is referred to the Web version of this article.)

Table 1
Data derived from N_2 gas adsorption/desorption adsorption measurement.

Sample	S_{BET} [a]	V_{micro} [b]	V_{TOT} [c]	V_{meso} [d]	d_{ave} [e]
	m^2/g	cm^3/g	cm^3/g	cm^3/g	nm
PA	483	0.31	1.74	1.43	14.4
CA	1016	0.42	1.53	1.11	6.0

[a] Apparent surface area from the BET model.
[b] Micropore volume from DR model.
[c] Total pore volume from N_2 adsorption.
[d] $V_{meso} = V_{TOT} - V_{micro}$.
[e] $d_{ave} = 4V_{TOT}/S_{BET}$.

spherical pores, while ca. 89% is confined to the wide channels.

The pore size distributions (Fig. 5b) were calculated by eq. (1) for the appropriate geometries. The pores, considered as spherical, has a characteristic diameter of ca. 30 nm (calculated on the basis of the melting process) and can be interpreted as water drops surrounded by the aerogel beads of 30 nm. Considering the slit-like pores or wide channels the distribution of the wall distance has a characteristic value of about 52 nm, but the pore size distribution is quite broad (derived from the freezing curve). Comparing this result with the SEM image of PA (Fig. 2a) we can conclude that the wide channels mean connected water layers between the aggregated beads in the macrostructure. These sizes are in the same range as the pore size distribution determined by N_2 adsorption experiments (Fig. 3c red dots). The broad size distributions extinguish the differences arising from the applied geometrical approaches of the two methods.

Summarizing the results of PA: micropores can be well detected with gas porosimetry, but are below the size limit of NMR cryoporometry; mesopores are detected similarly by both methods. We can state that the apparent mesopore structure does not significantly change in aqueous medium, but the cryoporometry could define two locations of different geometries and the distribution of water between them.

The structural changes of the aerogel after the carbonization (resulting in CA) have been also studied by NMR cryoporometry. As seen

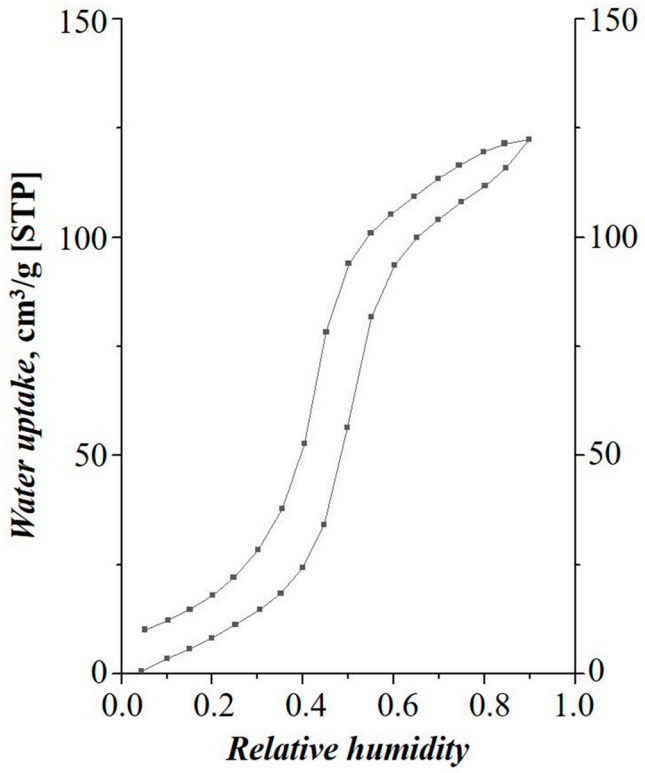

Fig. 4. Water vapor adsorption/desorption isotherms of the CA sample at 293 K.

in Fig. 6a the melting and freezing steps corresponding to the spherical pores cannot be detected any longer.

The freezing point depression characteristic for the wide channels remained, but the hysteresis became wider (ca. 2 K) indicating decreasing wall distance due to carbonization (Fig. 6a). As already mentioned, in the case of slit-like pores no melting-point depression is detectable, the heating process results in the melting point of bulk water [23,24]. However, the melting curve of CA is not as steep as expected at the bulk transition point (273.15 K), thus it indicates probably two melting processes. It leads to the conclusion that beside the wide channels another pore-geometry is present in the same temperature range, and the freezing and melting curves of the two geometries overlap. To model this phenomenon, we simulated the overlapping processes as seen in Fig. 6a. The measured freezing curve between 268 and 270 K, and the measured melting process up to 272.8 K show a hysteresis typical of cylindrical pores with $\Delta T_f/\Delta T_m \approx 2$, which is estimated with blue dashed lines. The melting curve of slit-like water was assumed steep at 273.1 K, while the freezing process was simulated from the remained measured points of the freezing curve, and signed with orange dot-and-dash lines. The total of the simulated freezing curves (green dotted line) well coincides with the measured points. From the maximum of the integrals the water amount in different geometries resulted in ca. 40% for slits and 60% for cylindrical pores, thus, the distribution of water in the confinements significantly changes after carbonization. The most frequent pore sizes of the slit-like and cylindrical pores are 28 and 36 nm respectively (Fig. 6b), which match the pore size distribution ranges obtained from the nitrogen adsorption experiment (slit geometry from NLDFT, Fig. 3b inset, and cylindrical from the BJH method, Fig. 3c). Nevertheless, we are aware that the two methods have differences in geometrical interpretations [23] and further experiments are needed for more definite conclusions.

Compared to the polymer aerogel the wall distance of the wide channels significantly decreased and the size-distribution is narrower in CA. It means that the aggregated beads got closer to each other as a result of the pyrolysis. Inside the aggregates cylindrical channels are assessed in the same size-range, instead of the spherical pores of PA. The distribution of water is more balanced between the two domains, indicating a pore network being more permeable for water molecules. There may be another reason which can contribute to the explanation of the structural differences: PA is a softer material than CA, therefore immersing the samples in water can give a different picture about the morphology from nitrogen porosimetry.

Since carbon aerogels have a hydrophobic carbon skeleton, cyclohexane as a non-polar probe liquid was also tested for CA. Two melting-freezing processes can be distinguished: one belongs to the bulk cyclohexane at 280 K, the other process shows a definite hysteresis with the ratio of $\Delta T_f/\Delta T_m = 2$, referring to cylindrical pores (Fig. 7a). The residual signal integral can be attributed to the remained frozen

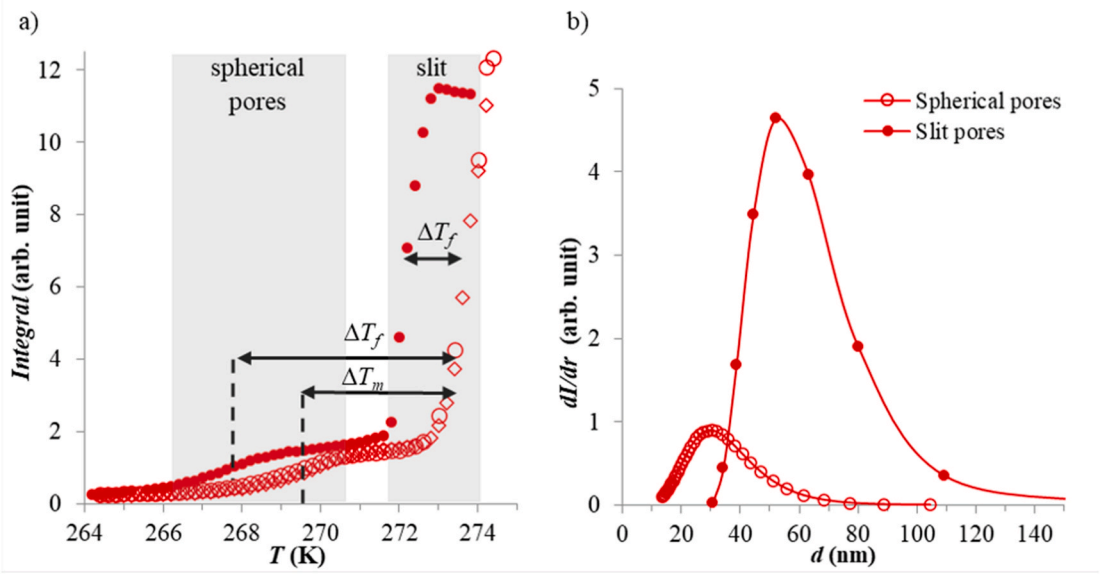

Fig. 5. a) Freezing (●) and melting (○,◊) curves of water in the PA sample. The different empty symbols show the reproducibility of the curves (second cycle). Double arrows show the melting (ΔT_m) and freezing point (ΔT_f) depressions. b) Pore size distributions of spherical (○) and slit-like (●) pores in PA. Solid lines are a guide to the eyes.

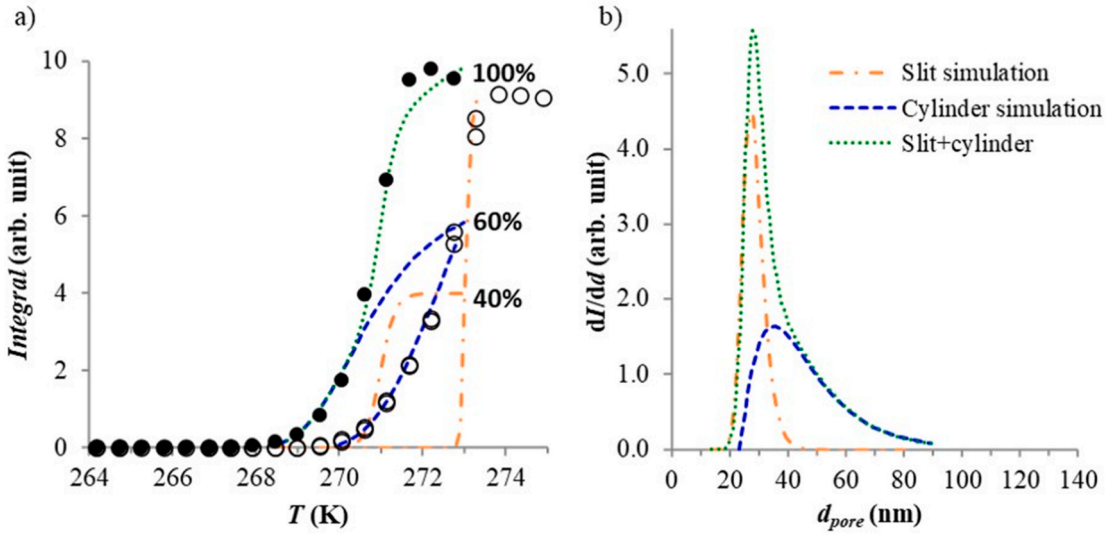

Fig. 6. a) Freezing (●) and melting (○) curves of water in the CA sample. Lines are simulated curves (details in text): dashed (blue) for cylinder geometry, dot-and-dash (orange) for slit geometry, while the dotted (green) line is their sum (freezing branches). Percentages show the contribution of the different geometries. b) Pore size distributions derived from the simulated freezing curves with the corresponding lines. (For interpretation of the references to colour in this figure legend, the reader is referred to the Web version of this article.)

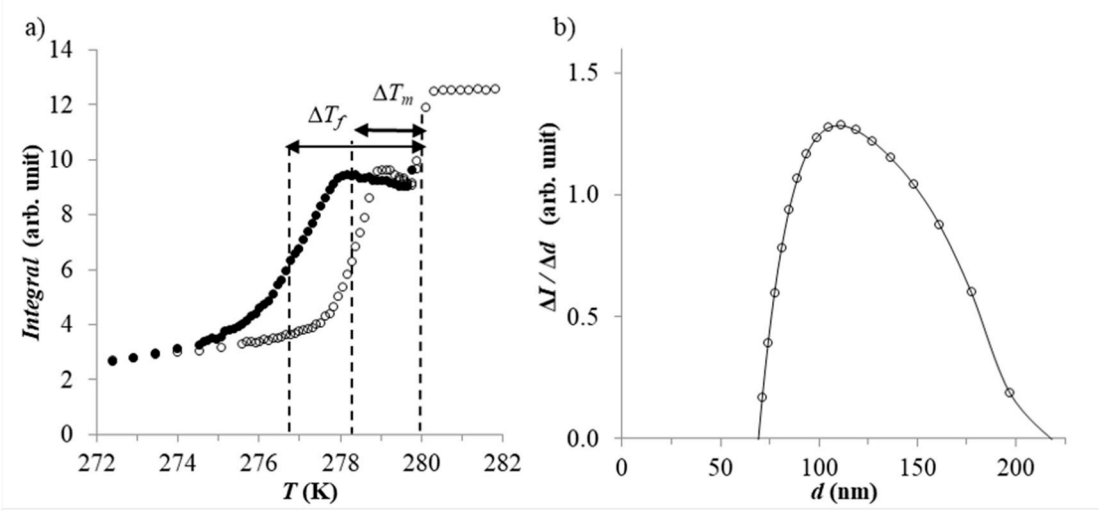

Fig. 7. a) Freezing (●) and melting (○) curves of cyclohexane in CA. b) Pore size distribution derived from the melting (○) curve with cylindrical geometry.

cyclohexane which is not relaxed during the applied echo time [23,45]. The broad pore size distribution has a maximum at diameter (d) ca. 110 nm (Fig. 7b) meaning that cyclohexane was detected in large, cylindrical channels. We assume that these correspond to the interconnected pore network among the aggregated particles of the aerogel structure.

There may be several factors that result in the difference of the pore morphology determined by the two probe liquids applied:

(i) According to a previous study, polymer-based carbons, with hydrophilic groups on their surface, show local swelling in non-polar solvents, like cyclohexane, with almost negligible macroscopic swelling [46]. It means that during the swelling the distance separating the beads of the aerogel structure decreases, *i.e.*, the pores shrink. This argument can explain why the mesopores of CA cannot be detected with cyclohexane and on the other hand, the observed macropores might be the result of the shrinkage of the larger macropores originally out of the scope of the technique (but seen in the SEM and TEM images, Fig. 2b–c).

(ii) There are hydrophilic groups (as seen from the water vapor adsorption isotherm) on the otherwise hydrophobic carbon skeleton. We presume that cyclohexane might not penetrate into the micropores and narrower mesopores if their inlet is blocked by the polar groups.

(iii) Another aspect is the unique behavior of cyclohexane as a probe liquid. For carbon-based materials it is advantageous that cyclohexane is hydrophobic. Its cryoporometric constant (K_c) is high, but also depends on the quality of the surface (we used a value from literature [23]). Below the transition temperature a plastic phase appears between the liquid and frozen crystalline states and the rotational diffusion of the molecules in the plastic phase results in the lengthening of the transverse relaxation time (T_2) [47]. This influences the NMR signal, thus the melting/freezing curves, and might affect the detection of cyclohexane in smaller confinements as well.

4. Conclusions

The objective of this work was a comparative analysis of aerogel

samples using a widely applied and well standardized method (vapor adsorption) and a recently adapted NMR technique (NMR cryoporometry). We found similarities and differences in the results. The pore structure of an RF polymer aerogel and its carbon aerogel derivative was investigated by low temperature nitrogen adsorption in vapor phase and NMR cryoporometry in liquid phase. Water and cyclohexane were used as polar and non-polar immersion media.

The comparison of the results shows that the two methods provide complementary information about the texture of the porous systems investigated. The microporous region can be explored by N_2 adsorption, in the mesopore size-range both techniques provide similar pore size distribution, while NMR cryoporometry expands the observation limit toward the macropore region. The combined application of the two methods allows a more detailed structural study of porous materials including the structural changes resulted from the carbonization and the occasional change of the morphology caused by the probe liquids.

It is demonstrated that the employment of carefully selected liquids, e.g., a polar and a non-polar solvent, may provide further information about the potential differences in gas and liquid media, bringing the characterization closer to the conditions of the real applications.

CRediT authorship contribution statement

Mónika Kéri: experimental work, data evaluation, Writing – original draft. **Balázs Nagy:** experimental work. **Krisztina László:** data evaluation, Writing – original draft. **István Bányai:** preliminary experiments, Conceptualization, Project administration.

Declaration of competing interest

The authors declare that they have no known competing financial interests or personal relationships that could have appeared to influence the work reported in this paper.

Acknowledgements

The research has been implemented with the support provided from the National Research, Development and Innovation Fund of Hungary, financed under the OTKA: K_131989 funding scheme. Mónika Kéri is grateful for the National Research, Development and Innovation Fund of Hungary (OTKA: PD_135169) for financial support. The research was also supported by the EU and co-financed by the European Regional Development Fund under the project GINOP-2.3.2-15-2016-00008 and VEKOP-2.3.2-16-2017-00013. The research reported in this paper and carried out at BME has been supported by the NRDI Fund (TKP2020 IES, Grant No. BME-IE-BIO) based on the charter of bolster issued by the NRDI Office under the auspices of the Ministry for Innovation and Technology. Some figures were created with BioRender.com.

References

[1] M. Schwan, R. Tannert, L. Ratke, New soft and spongy resorcinol-formaldehyde aerogels, J. Supercrit. Fluids 107 (2016) 201–208.
[2] J.P. Lewicki, C.A. Fox, M.A. Worsley, On the synthesis and structure of resorcinol-formaldehyde polymeric networks - precursors to 3D-carbon macroassemblies, Polymer 69 (2015) 45–51.
[3] S.A. Al-Muhtaseb, J.A. Ritter, Preparation and properties of resorcinol-formaldehyde organic and carbon gels, Adv. Mater. 15 (2) (2003) 101–114.
[4] A. Arenillas, J.A. Menéndez, G. Reichenauer, A. Celzard, V. Fierro, F.J. Maldonado-Hódar, E. Bailón, N. Job, Organic and carbon gels. From laboratory synthesis to applications. Book Series: Advances in Sol-Gel Derived Materials and Technologies, Springer, Berlin/Heidelberg, Germany, 2019.
[5] E. Frackowiak, F. Béguin, Carbon materials for the electrochemical storage of energy in capacitors, Carbon 39 (6) (2001) 937–950.
[6] C. Moreno-Castilla, F.J. Maldonado-Hódar, Carbon aerogels for catalysis applications: an overview, Carbon 43 (3) (2005) 455–465.
[7] L.W. Hrubesh, Aerogel applications, J. Non-Cryst. Solids 225 (1998) 335–342.
[8] Y. Zhu, H. Hu, W. Li, X. Zhang, Resorcinol-formaldehyde based porous carbon as an electrode material for supercapacitors, Carbon 45 (1) (2007) 160–165.
[9] N. Job, R. Pirard, J. Marien, J.-P. Pirard, Porous carbon xerogels with texture tailored by pH control during sol–gel process, Carbon 42 (3) (2004) 619–628.
[10] O. Czakkel, K. Marthi, E. Geissler, K. László, Influence of drying on the morphology of resorcinol–formaldehyde-based carbon gels, Microporous Mesoporous Mater. 86 (1) (2005) 124–133.
[11] C. Macías, P. Lavela, G. Rasines, M.C. Zafra, J.L. Tirado, C.O. Ania, On the correlation between the porous structure and the electrochemical response of powdered and monolithic carbon aerogels as electrodes for capacitive deionization, J. Solid State Chem. 242 (2016) 21–28.
[12] B. Nagy, I. Bakos, I. Bertóti, A. Domán, A. Menyhárd, M. Mohai, K. László, Synergism of nitrogen and reduced graphene in the electrocatalytic behavior of resorcinol - formaldehyde based carbon aerogels, Carbon 139 (2018) 872–879.
[13] H. Tamon, H. Ishizaka, T. Araki, M. Okazaki, Control of mesoporous structure of organic and carbon aerogels, Carbon 36 (9) (1998) 1257–1262.
[14] H. Tamon, H. Ishizaka, M. Mikami, M. Okazaki, Porous structure of organic and carbon aerogels synthesized by sol-gel polycondensation of resorcinol with formaldehyde, Carbon 35 (6) (1997) 791–796.
[15] V. Bock, A. Emmerling, J. Fricke, Influence of monomer and catalyst concentration on RF and carbon aerogel structure, J. Non-Cryst. Solids 225 (1998) 69–73.
[16] M. Mirzaeian, P.J. Hall, The control of porosity at nano scale in resorcinol formaldehyde carbon aerogels, J. Mater. Sci. 44 (10) (2009) 2705–2713.
[17] R. Kleinberg, Nuclear magnetic resonance, in: R. Celotta, T. Lucatorto (Eds.), Methods in the Physiscs of Porous Media, Academic Press1999, pp. 337-385.
[18] V.M. Gun'ko, V.V. Turov, Nuclear Magnetic Resonance Studies of Interfacial Phenomena, CRC Press, NewYork, 2013, pp. 455–522.
[19] D.T. Shane, R.L. Corey, C. McIntosh, L.H. Rayhel, R.C. Bowman, J.J. Vajo, A. F. Gross, M.S. Conradi, LiBH4 in carbon aerogel nanoscaffolds: an NMR study of atomic motions, J. Phys. Chem. C 114 (9) (2010) 4008–4014.
[20] F. D Orazio, S. Bhattcharja, J.C. Tarczon, W.P. Halperin, Magnetic resonance relaxation analyísis of porous media, in: J. Klafter, J.M. Draker (Eds.), Molecular Dynamics in Resricted Geometries, Wiley, New York, 1989.
[21] P.J. Barrie, Characterization of porous media using NMR methods, Annu. Rep. NMR Spectrosc. 41 (2000) 265–316.
[22] O.V. Petrov, I. Furó, Curvature-dependent metastability of the solid phase and the freezing-melting hysteresis in pores, Phys. Rev. 73 (2006), 011608.
[23] O.V. Petrov, I. Furó, NMR cryoporometry: principles, applications and potential, Prog. Nucl. Magn. Reson. Spectrosc. 54 (2) (2009) 97–122.
[24] O. Petrov, I. Furó, A study of freezing–melting hysteresis of water in different porous materials. Part II: surfactant-templated silicas, Phys. Chem. Chem. Phys. 13 (36) (2011) 16358–16365.
[25] O. Petrov, I. Furó, A study of freezing–melting hysteresis of water in different porous materials. Part I: porous silica glasses, Microporous Mesoporous Mater. 138 (1) (2011) 221–227.
[26] C. Cadar, C. Cotet, L. Baia, I. Ardelean, Probing the connectivity and wettability of carbon aerogels and xerogels via low-field NMR, AIP Conference Proceedings 2017 (1) (1917), 040006.
[27] C. Cadar, C. Cotet, L. Baia, L. Barbu-Tudoran, I. Ardelean, Probing into the mesoporous structure of carbon xerogels via the low-field NMR relaxometry of water and cyclohexane molecules, Microporous Mesoporous Mater. 251 (2017) 19–25.
[28] S. Ghosh, K.V. Ramanathan, A.K. Sood, Water at nanoscale confined in single-walled carbon nanotubes studied by NMR, Europhys. Lett. 65 (5) (2004) 678.
[29] Y. Zhao, Y. Sun, S. Liu, K. Wang, Y. Jiang, Pore structure characterization of coal by NMR cryoporometry, Fuel 190 (2017) 359–369.
[30] M. Krutyeva, F. Grinberg, F. Furtado, P. Galvosas, J. Karger, A. Silvestre-Albero, A. Sepulveda-Escribano, J. Silvestre-Alberto, F. Rodriguez-Reinoso, Characterization of carbon materials with the help of NMR methods, Microporous Mesoporous Mater. 120 (1–2) (2009) 91–97.
[31] R.W. Pekala, Organic aerogels from the polycondensation of resorcinol with formaldehyde, J. Mater. Sci. 24 (9) (1989) 3221–3227.
[32] O. Czakkel, E. Székely, B. Koczka, E. Geissler, K. László, Drying of resorcinol–formaldehyde gels with CO2 medium, Microporous Mesoporous Mater. 148 (1) (2012) 34–42.
[33] S. Brunauer, P.H. Emmett, E. Teller, Adsorption of gases in multimolecular layers, J. Am. Chem. Soc. 60 (2) (1938) 309–319.
[34] M.M. Dubinin, L.V. Radushkevich, The Equation of the Characteristic Curve of Activated Charcoal, Chem. Zentr., 1947, pp. 875–890.
[35] E.P. Barrett, L.G. Joyner, P.P. Halenda, The determination of pore volume and area distributions in porous substances. I. Computations from nitrogen isotherms, J. Am. Chem. Soc. 73 (1) (1951) 373–380.
[36] J.H. Strange, M. Rahman, E.G. Smith, Characterization of porous solids by NMR, Phys. Rev. Lett. 71 (21) (1993) 3589–3591.
[37] W.P. Halperin, F. D Orazio, S. Bhattacharja, C.J. Traczon, Magnetic resonance relaxation analysis of porous media, in: J. Klafter, J.M. Drake (Eds.), Molecular Dynamics in Restricted Geometrics, Wiley, New York, 1989, p. 331.
[39] R.M.E. Valckenborg, L. Pel, K. Kopinga, Combined NMR cryoporometry and relaxometry, J. Phys. Appl. Phys. 35 (3) (2002) 249.
[40] C. Ammann, P. Meier, A. Merbach, A simple multinuclear NMR thermometer, J. Magn. Reson. 46 (2) (1969) 319–321, 1982.
[41] D. Kehl, B. Sipos, A telítödési, a logisztikus és az életgörbe alakú trendfüggvények becslése Excel parancsfájl segítségével, Statisztikai Szle. 87 (4) (2009) 381–411 (in Hungarian).
[42] M. Thommes, K. Kaneko, V. Neimark Alexander, P. Olivier James, F. Rodriguez-Reinoso, J. Rouquerol, S.W. Sing Kenneth, Physisorption of gases, with special reference to the evaluation of surface area and pore size distribution (IUPAC Technical Report), Pure Appl. Chem. (2015) 1051.

[43] B. Nagy, I. Bakos, E. Geissler, K. László, Water-ionic liquid binary mixture tailored resorcinol-formaldehyde carbon aerogels without added catalyst, Materials 12 (24) (2019) 4208.
[44] B. Nagy, S. Villar-Rodil, J.M.D. Tascón, I. Bakos, K. László, Nitrogen doped mesoporous carbon aerogels and implications for electrocatalytic oxygen reduction reactions, Microporous Mesoporous Mater. 230 (2016) 135–144.
[45] F. Zhu, W. Hu, J. Cao, B. Liu, Y. Liu, C. Chang, Probe material choice for nuclear magnetic resonance cryoporometry (NMRC) measurements of the nano-scale pore size distribution of unconventional reservoirs, Energy Explor. Exploit. 37 (1) (2019) 412–428.
[46] K. László, O. Czakkel, K. Josepovits, C. Rochas, E. Geissler, Influence of surface chemistry on the SAXS response of polymer-based activated carbons, Langmuir 21 (18) (2005) 8443–8451.
[47] J.B.W. Webber, Studies of nano-structured liquids in confined geometries and at surfaces, Prog. Nucl. Magn. Reson. Spectrosc. 56 (1) (2010) 78–93.